Available online at www.CivileJournal.org

Civil Engineering Journal

(E-ISSN: 2476-3055; ISSN: 2676-6957)

Vol. 11, No. 12, December, 2025

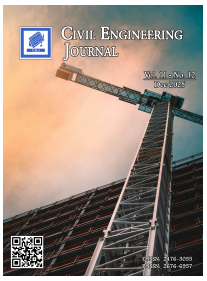

Three-Dimensional Finite Element Evaluations of H-Steel Beams Strengthened with Various Types of Steel Stiffeners

Ali F. Atshan [1], Mohammed A. Radi [1], Ali Kifah Kadhum [1], Malik H. Assi [1*], Zuhair Abd Hacheem [1], Noor S. Taresh [2]

[1] *Department of Water Resources Engineering, College of Engineering, Mustansiriyah University, Baghdad, Iraq.*

[2] *Department of Highways and Transportation Engineering, College of Engineering, Mustansiriyah University, Baghdad, Iraq.*

Received 24 August 2025; Revised 15 November 2025; Accepted 21 November 2025; Published 01 December 2025

Abstract

Three-dimensional finite element analyses were carried out to assess the impact of various types of lateral stiffeners on the response of steel beams. Hot-rolled simply supported H-steel beams were modeled in Abaqus and strengthened with centrally located vertical, V-shaped, inverted V-shaped, single X-shaped, or doubled X-shaped stiffeners. All these stiffeners possess a similar quantity of steel by varying the length and thickness of the stiffeners. The behavior of beams was studied in the elastic phase, hardening phase, necking phase, and failure. The yield stress, ultimate load, deflection value, and hardening in the three phases were also examined. It has been found that the findings indicate that altering the configuration of the stiffener, while maintaining its location and steel volume, can influence the response of the strengthened beam either favorably or adversely. Two stiffeners raised the yield load by 9.6%, the ultimate load by 10.8%, and elastic storage energy by 70% above the reference beam. One kind of stiffener increases in the plastic region, two types drop somewhat, and two others decrease significantly. The necking region shows a rise of 237% in one threshold and 36% to 90% for the other beams compared to the reference beam. Furthermore, the software provides a definitive indication of the kind of stiffener and the degree of its advantage, while simultaneously revealing the type of stiffener that is not advantageous.

Keywords: Strengthened; Stiffeners; Finite Element; Abaqus; Deflection Response; Toughness; Elastic Region; Plastic Region; Necking Region; Yield Stress; Ultimate Stress.

1. Introduction

Steel buildings need to be strengthened just as much as concrete structures or any other aged construction. The full moment capacity of steel beams may be attained if local and lateral buckling are inhibited. Lateral buckling may be alleviated by applying enough suppression to the compressive flange. Furthermore, beams may experience failure owing to local buckling shown as shear yielding, localized web denting, or deformation of slender flanges. These flaws may be mitigated by using supplementary flange plates [1]. Atshan et al. (2024) investigated the impact of altering the strand position (modifying the eccentricity value) on the performance of steel beams, observing that the stiffness of the beams escalates with an increase in eccentricity [2]. Yang & Lui (2012) have examined steel beams strengthened with inclined stiffeners, finding that these modifications substantially boost the lateral torsional buckling capability of the beams. The extent of this enhancement is mostly determined by the positioning of the stiffeners and the unsupported lateral span of the beam. Moreover, the beneficial impacts of inclined stiffeners are amplified in longer beams and with an increase in the degree of inclination [3]. Prabha & Emilreyan (2018) analyzed the performance of I-section steel beams strengthened

* Corresponding author: malik_habeeb@uomustansiriyah.edu.iq

http://dx.doi.org/10.28991/CEJ-2025-011-12-06

with horizontal, vertical, and inclined stiffeners in different configurations throughout the beam's length. Their research has shown a significant reduction in deflection and an enhancement in failure load [4]. Al-Ridha et al. (2020) determined that including supplementary plates to the upper and lower flanges of a beam, together with inclined stiffeners, enhances its stiffness relative to a reference beam, as shown by the load-strain and load-deflection responses. The stiffening effect is enhanced with a greater width of the supplementary steel plates. Their findings indicated that including both supplementary plates and inclined stiffeners transformed the failure mechanism from 'lateral buckling' to a 'plastic hinge' that developed under the concentrated load at mid-span [5].

Al-Ridha et al. (2019) increased the failure load by strengthening steel beams using carbon fiber. In addition, they discovered that the failure load increased and the beams were stiffer when carbon fiber was used in conjunction with a reduction in beam length [6]. Al-Ridha et al. (2020) have enhanced beams by including supplementary plates and carbon fiber strips, resulting in a significant increase in failure load capacity and increased stiffness of the beams [7]. The study examined the impact of longitudinal stiffener length, transverse stiffener length, combined longitudinal and transverse stiffeners, double transverse stiffeners, bearing depth, and bearing length, revealing that these factors altered failure modes and substantially enhanced the capacity of the coped beam specimens [8]. Siwowski & Siwowska (2018) have examined the flexural behavior of steel beams augmented by CFRP strips. A comparison was conducted between two reinforcement systems: the first involves beams reinforced with carbon fiber and glue, while the second use pre-stressed strips for reinforcement [9]. Peiris & Harik (2021) used steel beams reinforced with 50 mm wide UHM CFRP strip panels, resulting in an enhancement of the failure load [10]. The dimensions of the cover plate, including its length and area, together with the suggested welding method used to weld the cover plate under load, significantly influence the enhancement of the ultimate load-bearing capacity of the examined specimens [4, 11]. The test findings of the beams suggest that the width-to-thickness ratio of the bonded plate must surpass 20, and to provide good adhesion, both the beam and plate surfaces must be meticulously cleaned using suitable procedures. The bonding procedure must be conducted with utmost precision [12]. Sallam et al. (2005) found that terminal fixation should be implemented on the bonded plate situated on the tension side of the beam. They have also determined that using a plate secured on the pressure side is unsuccessful. To strengthen the compressive side, an extra plate must be bonded to the original beam via a continuous welding procedure, as referenced in [13].

Al-Ridha et al. (2020) [7] and Haghani et al. (2009) [14] have examined the efficacy of reinforcing steel beams using vertical stiffeners and carbon fiber. Yousef (2015) concluded from experimental data that the ultimate load capacity of beams was affected by the length of the cover plate. The impact was diminished when the cover plate's area was less than that of the flange. Extending the cover plate's length from 36% to 50% has resulted in a 1% to 5% enhancement in ultimate capacity. Nonetheless, altering the design of the cover plate while preserving the same length did not affect the eventual capacity, as shown in reference [15]. Demir et al. (2018) have examined the situation of reinforcing beams using external steel clips and longitudinal reinforcements. The use of clips alone did not significantly affect the failure load capacity of the tested concrete beams; however, ductility increased approximately tenfold, and the failure behavior transitioned from brittle to ductile [16]. Chen & Sudibyo (2018) have examined the efficacy of internal stiffeners, including midspan stiffeners and plastic hinge-zone stiffeners, in enhancing composite action and flexibility of the reinforced beams [17]. Yang et al. (2025) investigated reinforced I-steel beams produced by wire arc additive manufacturing (WAAM), resulting in enhanced beam performance characterized by improved ultimate moment tolerance and increased stiffness [18]. Yuan et al. have investigated the reinforcement of reinforced concrete beams through the use of high-strength steel wire and highly ductile engineered cementitious composites (ECC) [19]. Karande & Anjalekar (2016) performed research demonstrating that an increase in the flange slenderness of I-section beams diminishes both moment-carrying capacity and curvature ductility [20]. Truong et al. (2019) found that the enhancement in the ultimate strength of the beam (with web slenderness up to 350) varies from a minimum of 8% to a maximum of 104.41%. Moreover, it attains its peak when the thinness of the fabric and edges is diminished [21]. Using finite element modeling, Han et al. (2008) was able to reasonably predict the relationship between the lateral load and lateral displacement of a composite frame and the maximum lateral load-bearing capacity [22].

Gardner L. et al. (2024) reinforced columns using Wire Arc Additive Manufacturing (WAAM), applying three variations to the flange, resulting in enhanced structural efficiency relative to their counterparts. The three methods used to boost strength were increased area, second area moment, enhanced local buckling resistance, and a more favorable residual stress distribution. Of the various strengthening procedures analyzed, the specimens reinforced with stepwise sinusoidal-shaped stiffeners at the flange tips demonstrated the highest improvements in structural efficiency [23]. Jagtap et al. (2024) performed a reinforcement of steel sections using first-pass CFRB stiffeners and second-pass steel stiffeners. It has been found that using both stiffeners prevented localized failure of the upper flange of the beams. The results also showed convergence [24]. Yang et al. (2025) showed that strengthening beams using WAAN may result in some undesirable increases compared to bare beams. However, strengthening using WAAN improved the mechanical properties of rolled steel, resulting in significant increases in bending moments ranging from 31% to 84% for the strengthened beams [25]. Xie et al. (2025) reinforced I-steel beams with side plates, and this strengthening showed an increase in the resistance to lateral torsional buckling [26].

2. Research Methodology

Figure 1 illustrates a systematic approach to studying how various stiffeners of different shapes affect beam behavior until collapse. A reference model, without stiffeners, and five models with varying stiffeners were developed using the Abaqus software in this study. Next, the characteristics of the study's models and explained the loading procedure were demonstrated. The models' load-deflection curves, toughness, and beam behavior in the elastic, hardening, and post-ultimate regions were then obtained and analyzed.

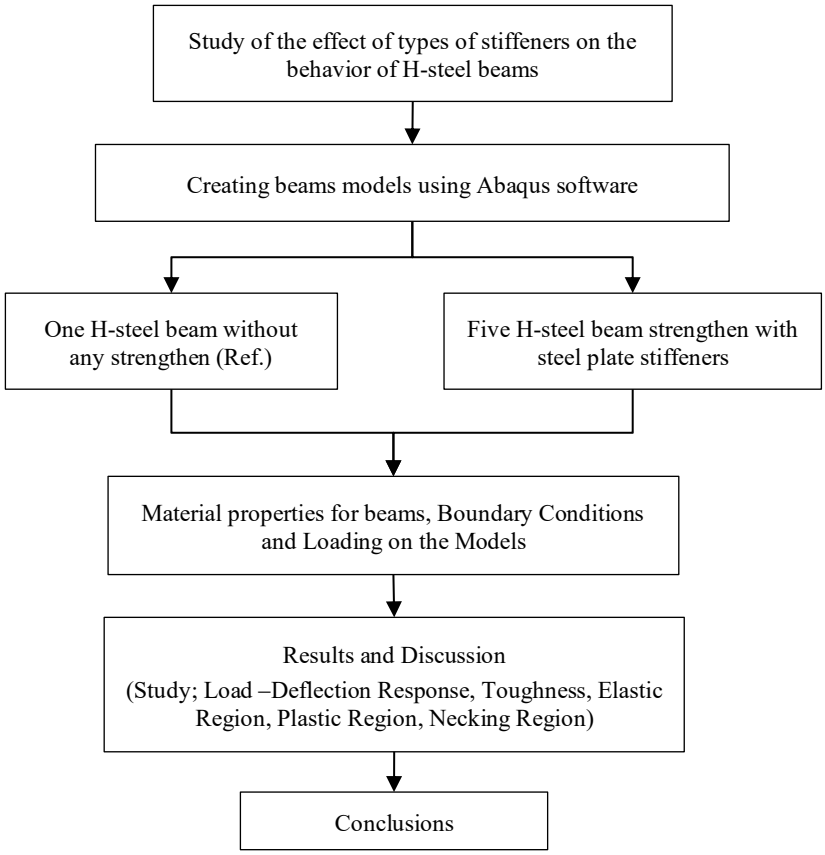

Figure 1. Methodology of the study

2.1. Research Significance

This research aims to assess the efficacy of various types of lateral stiffeners, connected to the web laterally, the upper flange inferiorly, and the lower flange superiorly. It will examine their impact on yield load, maximum load, failure load, and their influence on beam deformation from the onset of loading to the yield point, as well as in the strain hardening region from the yield point to the maximum load, and the behaviour of beams post-maximum.

3. Finite Element Model

3.1. General Descriptions

In this research, the models were made using a hot-rolled steel beam (H-Beam) of size (248×124) mm, with a total length of 3000 mm and an effective length of 2900 mm as shown in Figure 2. The cross-sectional dimensions and properties of the models are shown in Table 1.

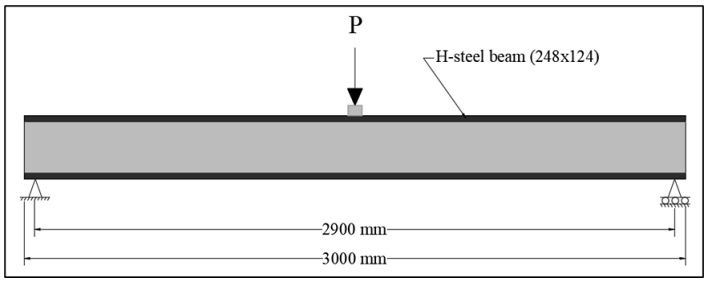

Figure 2. Typical steel beam details

Table 1. Dimensions and properties of steel beams cross section

Dimensions (mm)	Radius of curvature (mm)	Cross sectional area (mm^2) $\times 10^2$	Mass per meter (kg/m)	Moment of inertia ($mm^4 \times 10^4$)	Yielding strength (f_y) (MPa)	Ultimate tensile strength (f_u) (MPa)	
H = 248	r = 12	32.68	25.7	Ix-x = 3540	362	513	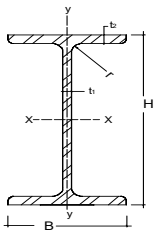
B = 124							
t_1 = 5				Iy-y = 255			
t_2 = 8							

A comprehensive description of the *modelled beams* is provided below:

- Beam (A0) serves as the reference beam; it is a steel section devoid of any reinforcements or modifications.
- The beam (A01) is identical to the reference beam in terms of steel section and is reinforced with vertical stiffeners measuring (20 × 59.5 × 232) mm, positioned at the midpoint (beneath the concentrated load) and at the supports.
- The beam (A02): the vertical stiffener at the center of the beam was substituted with two inclined stiffeners (7×59.5×328 mm), positioned at a 45-degree angle in the form of an inverted letter V, utilizing the same steel dimensions as the original vertical stiffener.
- The beam (A03) is identical to beam (A02), with the distinction that the two inclined stiffeners are configured in a V shape.
- The two inclined stiffeners were substituted with two X-shaped stiffeners measuring (3.5×59.5×328) mm on each side, maintaining the same dimensions as the steel utilized in the prior beams.
- The beam (A05): The four inclined stiffeners were replaced with two stiffeners (7×59.5×328) mm configured in a 'X' shape at the midpoint of the beam, positioned on each side of the web. The dimensions of the beam stiffeners are presented in Table 2. Figure 3 illustrates the shape of beams.

Table 2. Dimensions of stiffeners of the beams

BEAM	No. of vertical stiffener	Dim. of vertical stiffener (mm)	Inclined stiffener	Dim. of inclined stiffener (mm)
A0	0	-	0	-
A01	6	232×59.5×20	0	-
A02	4	232×59.5×20	4	328×59.5×7
A03	4	232×59.5×20	4	328×59.5×7
A04	4	232×59.5×20	8	328×59.5×3.5
A05	4	232×59.5×20	4	328×59.5×3.5

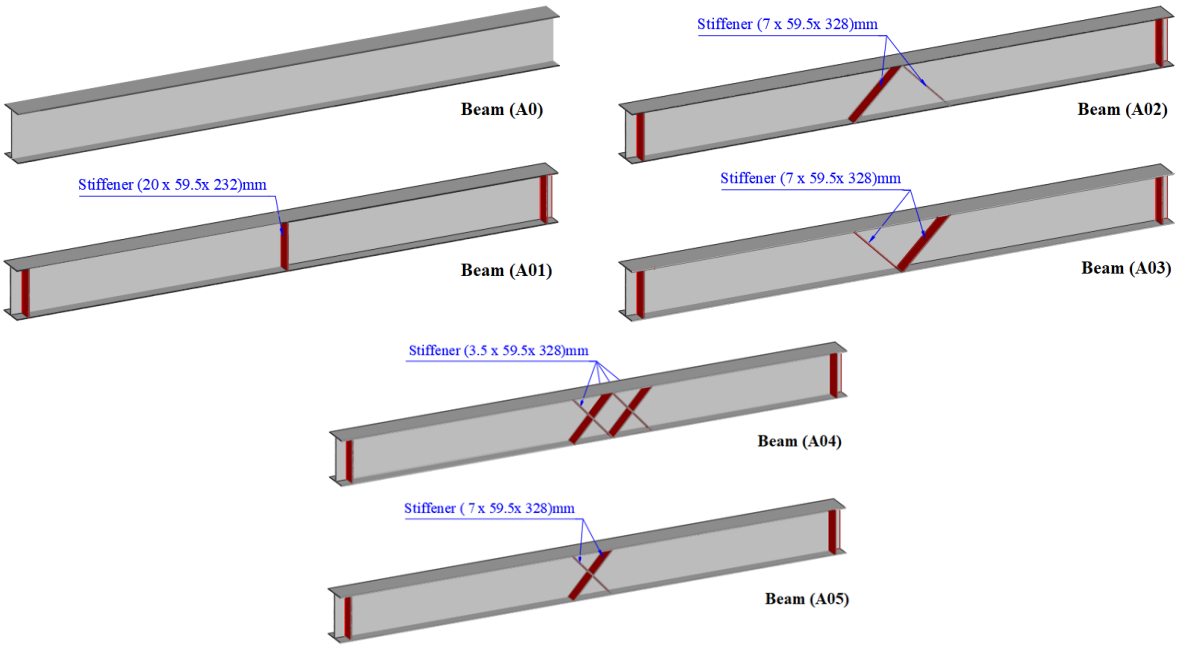

Figure 3. Detailing of the beams

3.2. Boundary Conditions and Loading on the Model

All modelled beams were simply supported by a roller support on one side and a hinged support on the opposite side. Two plates were affixed to the lower flange of the steel beam to mitigate stress concentration. One plate was anchored as a hinge, while the other was secured as a roller by imposing limitations along their central axis. All modeled beams were simply supported by a roller support on one side and a hinged support on the opposite side. Two plates were affixed to the lower flange of the steel beam to mitigate stress concentration. One plate was anchored as a hinge, while the other was secured as a roller by imposing limitations along their central axis. In this study, the probability of failure for beams was directed towards a plastic hinge by restricting it from rotating about the longitudinal axis of the beam (Z-axis) at three points at the supports and in the middle, but this restriction is not sufficient to prevent lateral buckling failure in the region between the supports and the middle of the beam.

Since this is theoretical research, it is difficult to predict the failure load of the models. However, it is possible to calculate the total vertical deflection of the models theoretically for the elastic and plastic regions. The concentrated load was applied gradually in the middle of the beam as a vertical deflection, and accordingly, the total vertical deflection was calculated (until the collapse of the reference beam), as shown below:

The total deflection of the reference beam up to failure can be determined, assuming the yield stress is 362 MPa, the modulus of elasticity (E) is 200,000 MPa, the effective beam length is 2,900 mm, and the total cross-sectional area is 3,268 mm². The load resulting in the plastic hinge was calculated using the methodology of Salmon et al. [27]. As shown in Equations 1 to 3.

1- Compute Plastic Section Modulus (Z)

$$Z = \sum(A_i . y_i)$$
$$Z = 2(124\times8\times120) + (116\times5\times58) = 271720 \text{ mm}^3 \quad (1)$$

2- Plastic Moment (M_P)

$$M_P = f_y . Z$$
$$M_P = 362 \times 271720 = 98362640\ N.mm \quad (2)$$

3- For Concentrated One-Point Load

$$P = \frac{4M_P}{L}$$
$$P = \frac{4\times98362640}{2900} = 135672.6\ N \quad (3)$$

P≃135.7 kN (the ultimate load causes the failure in plastic hinge), where A_i is area in elastic section, y_i is centroidal distance from the neutral axis, and f_y yield strength of material.

In this study, the load is applied as a vertical displacement, and it is essential to determine the deflection value from the first application of the load until failure occurs. The vertical deflection is computed in two phases. The first phase corresponds to the elastic zone, as seen in Equation 4 [28]:

$$\delta_{elastic} = \frac{P_y L^3}{48EI}$$
$$\delta_{elastic} = \frac{138\times10^3\times2900^3}{48(2\times10^5)(3540\times10^4)} \quad (4)$$
$$\delta_{elastic} = 11{,}73\ MM$$

The second phase signifies the plastic zone. The vertical deflection of the beam at this point may be approximately computed based on the plastic joint rotation (θp), as shown in Equation 5 [29]. The rotation of the plastic hinge (θp) value for a reference beam on the verge of collapse according to specification (FEMA-356 and FEMA-440) for the section used in the research is 0.127 rad [29]. If (θp) is set at 0.127 rad, the vertical deflection in the plastic zone for the reference beam (A0) is basically 184.15 mm.

$$\delta_p = \theta_p \times \frac{L_{eff}}{2}$$
$$\delta_p = 0{,}127 \times \frac{2900}{2} = 184{,}15\ mm \quad (5)$$

Total vertical deflection for the reference beam (on the verge of collapse) (δ elastic + δ plastic) = 11.73+184.15 = 195.88 mm. To give a broader idea of the beam's behavior, the beam behavior was studied up to 300 mm, i.e. approximately θp = 0.2 rad.

3.3. Material Properties

This work studied the geometric and nonlinear material characteristics of steel beams using a three-dimensional finite element model. Von Mises yield criteria were employed in nonlinear analysis. The steel beam was simulated using S4R shell components. To ensure numerical solution accuracy, the same mesh size was employed to analyze H-steel. The hot-rolled steel section H248×124 has a mass per meter of 25.7kg for SS400, with a modulus of elasticity (E) of 2×105 MPa, yielding strength (Fy) of 362 MPa, and ultimate tensile strength (Fu) of 513 MPa [2] This research used ABAQUS' plastic option to mimic steel's elastic–plastic properties. To correctly describe steel's nonlinear reaction under loading, this material description accepts a bilinear or multilinear stress–strain relationship. This model approximated H-shaped steel beams and steel plates (stiffeners). For this investigation, Modulus of elasticity (Es) was set at 200000 N/mm² and passion's ratio (vs) was set at 0.3, typical for structural steel. The Equations 6 to 8 regulate the stress-strain curve from loading to the yield point and subsequently to failure via the ultimate stress [30, 31].

$$\sigma_s = \begin{cases} E_s\varepsilon & for\ \varepsilon \le \varepsilon_y \\ f_y & for\ \varepsilon_y < \varepsilon \le \varepsilon_{sh} \\ f_y + (f_u - f_y)\left\{0{,}4\left(\frac{\varepsilon-\varepsilon_{sh}}{\varepsilon_u-\varepsilon_{sh}}\right) + 2\left(\frac{\varepsilon-\varepsilon_{sh}}{\varepsilon_u-\varepsilon_{sh}}\right) / \left[1 + 400\left(\frac{\varepsilon-\varepsilon_{sh}}{\varepsilon_u-\varepsilon_{sh}}\right)^5\right]^{1/5}\right\} & for\ \varepsilon_{sh} < \varepsilon \le \varepsilon_u \end{cases} \quad (6)$$

$$\varepsilon_u = 0{,}6\left(1 - \frac{f_y}{f_u}\right)\ but\ \varepsilon_u \ge 0{,}06\ for\ hot-rolled\ steel \quad (7)$$

$$\varepsilon_{sh} = 0{,}1\left(\frac{f_y}{f_u}\right) - 0{,}055 \quad but \quad 0{,}015 \le \varepsilon_u \le 0{,}03 \quad (8)$$

where, σ_s is stress in steel beam, ε is strain, ε_{sh} strain hardening strain, ε_u is strain at ultimate stress, ε_y yield strain.

4. Results and Discussion

4.1. Effect of Using Stiffeners on Load–Deflection Response

Figures 4 and 5, together with Table 3, depict the load-deflection characteristics of beams A0, A01, A02, A03, A04, and A05. The slope of the beams up to the yield load is nearly identical. Beams (A04 and A05) demonstrated a 9.6% increase in yield load compared to the reference beam, while beam (A04) achieved an increase of 10.28% in maximum load relative to the reference beam. It may be noted that in all beams (A0, A01, A02, A03, A04, and A05), the amount of increase in the vertical deflection at the maximum load is greater by 8.8, 10.3, 6, 2.3, 6.1, and 1.9 times than at the yield load, according to the sequence. The worst behavior is observed in beams A03 and A05 in the strain hardening region, where the vertical deflection values are similar, indicating that stress concentration occurs in a specific area, leading to a quicker attainment of maximum load.

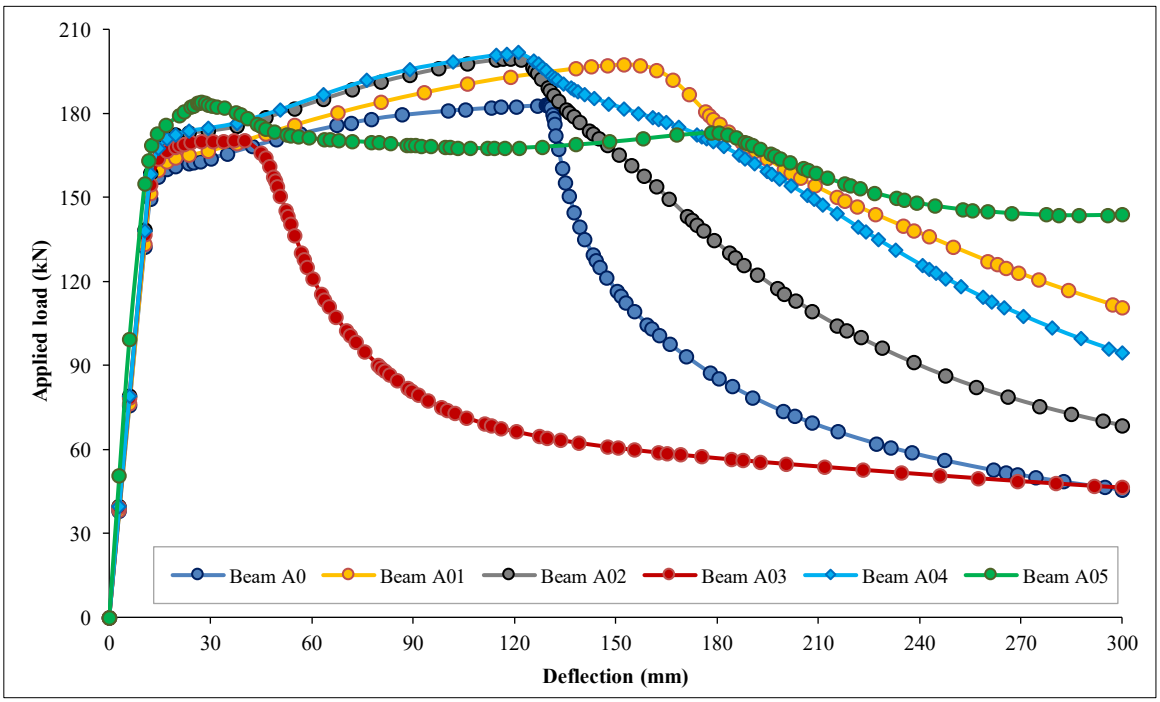

Figure 4. Load-deflection curves of beams

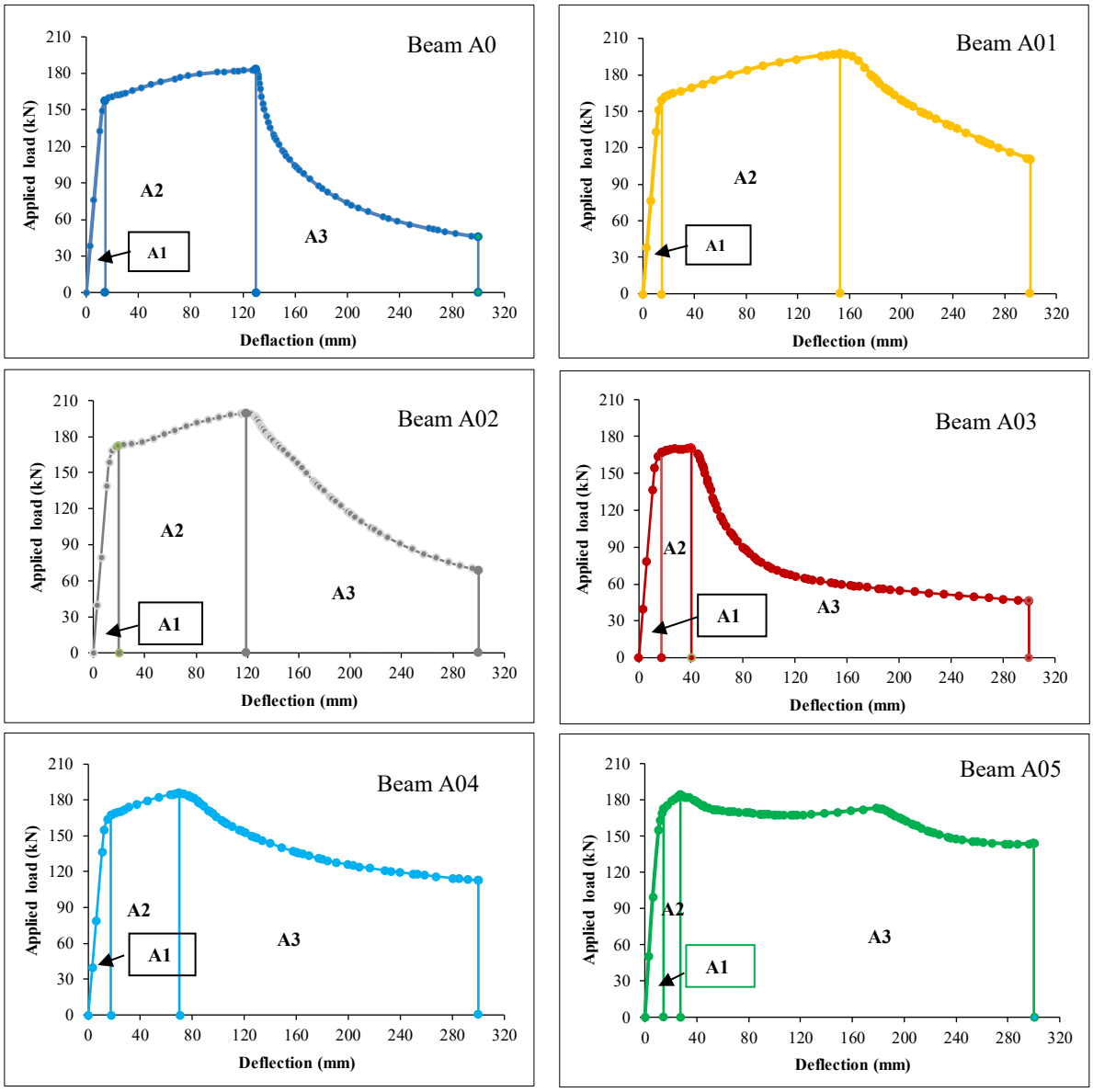

Figure 5. Area under curve for load-deflection for all beams

Table 3. Ultimate and yielding load of beams

Beam symbol	Yield Load (*fy*) (kN)	% of increase in compared to ref.	Deflection at Yield Load (mm)	Ultimate load (*fu*) (kN)	% of increase in compared to ref.	Def. in beam at Ultimate load	% of increase in compared to ref.	Load at def. 300 mm
A0	157.424	-	14.71875	182.923	-	129.8373	-	45.5823
A01	159.601	1.4	14.71875	197.367	7.9	152.612	17.5%	110.734
A02	172.221	9.4	19.78125	199.487	9.05	118.9746	-8.3%	68.6278
A03	166.628	5.85	17.25	170.269	-6.9	40.308	-68.95	46.3554
A04	172.514	9.6	19.78125	201.736	10.28	121.1103	-6.71	94.5409
A05	172.547	9.6	14.4375	184.006	0.6	27.45372	-78.85	143.896

It is also noticed in Figure 4 that in all curves there is a fracture that varies in strength according to the type of strengthening. The reason for this is the occurrence of buckling failure in the section (either in the flange, the web, or both), which causes the beam to fail faster than expected.

4.2. Toughness of the Beams

A comparison of beams strengthened with different types of stiffeners can be conducted by calculating the area under the curve, as illustrated in Figure 5 and Table 4. A larger area correlates with an increased load-bearing capacity and enhanced performance under load for the beam. The region beneath the curve is segmented into three distinct sections. The initial stage commences at the onset of loading and continues until the yield point is attained. This phase signifies the elastic stage, during which elastic deformation takes place in the subjected material. The deformity disappears when

the load is removed. Figure 5 and Table 4 indicate that beam A01 possesses the largest area, measuring 1550.6 kN.mm, which represents a 5.74% increase relative to the reference beam A0. Stage two commences from the yield point and progresses to the ultimate load. At this stage, the area under the curve indicates the beam's capacity to endure deformations beyond the yield point without failure. The beam (A02) is deemed superior at this stage, with an area under the curve measuring 25223.985 kN.mm, representing a 25.6% increase relative to the reference beam (A0). It may be noted that in the two beams (A03, A05) there is a large decrease in area by 80.5438% and 88.3882%. The reason for these decreases is the concentration of stresses in certain areas, which leads to a rapid arrival at the maximum load, which in turn leads to a sharp flange failure and a buckling in the web. The third stage extends from the ultimate load point to the failure point. The softening stage denotes the energy absorbed prior to failure. A reduction in this area correlates with an increased rate of beam failure, and conversely, an increase in area corresponds to a slower failure rate. At this stage, beam A05 is identified as the optimal choice, exhibiting an area of 44,335 and an increase rate of 237.6% compared to the reference beam. The larger the area, the greater the warning before the collapse.

Table 4. The area under curve value for beams (A0, A01, A02, A03, A04 and A05)

Beam symbol	From zero to yield point (kN.mm)	% of increase in compare to ref.	From yield point to ultimate load (kN.mm)	% of increase in compare to ref.	From ultimate load to load at Def. 300 mm (kN.mm)	% of increase in compare to ref.	Total area under load-deflection curve
A0	1321.8187	-	20083.906	-	13131.77	-	34537.495
A01	1335.2372	51.01	25223.985	25.59302	21892.643	66.7151	48451.865
A02	2253.7935	70.5	18505.834	-7.8574	21461.039	63.42838	42220.666
A03	1786.2312	35.31	3907.563	-80.5438	17865.558	36.04836	23559.353
A04	2251.599	70.34	19083.38	-4.98173	25063	90.85774	46397.98
A05	1526.85	15.5	2332.10	-88.3882	44335.01	237.6164	48193.97

4.3. Effect strengthen the Beams by Stiffeners on Yield Stress in Beams

In Figure 6, it is noted that in all beams, the larger the width of the stiffeners, the more the stresses are distributed over a larger area (meaning that it leads to a redistribution of stresses over a larger area, which leads to an increase in the value of bearing the applied loads). It may be noted that the stress in all beams' values at the yield point ranges from 372 to 412 MPa. It is clear to us that the amount of stress in the beams depends on the slenderness of the stiffeners and their location. The thinner the stiffeners and the closer the stiffener is to or under the concentrated load, the greater the amount of stress. It is clear to us that the amount of stress in the beams depends on the thinness of the stiffeners and their location. The thinner the stiffeners and the closer the stiffener is to or under the concentrated load, the greater the amount of stress.

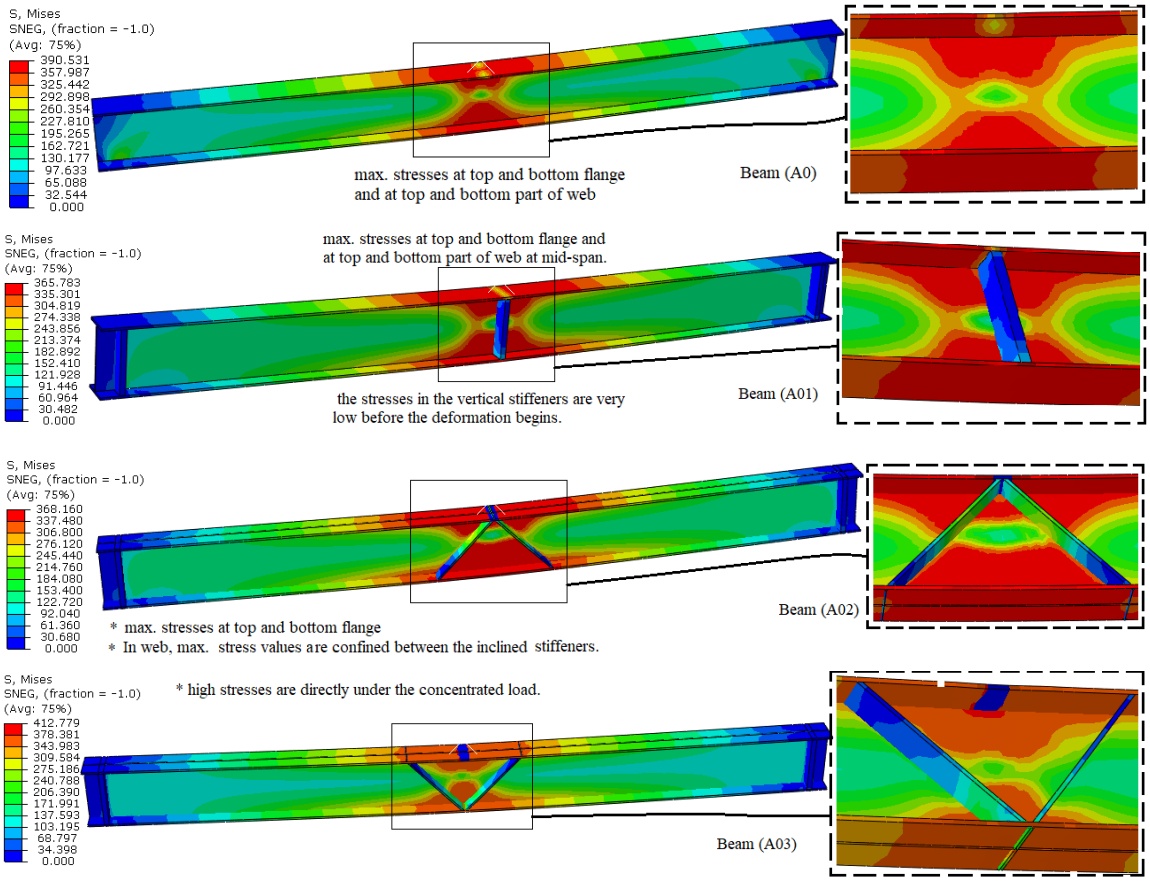

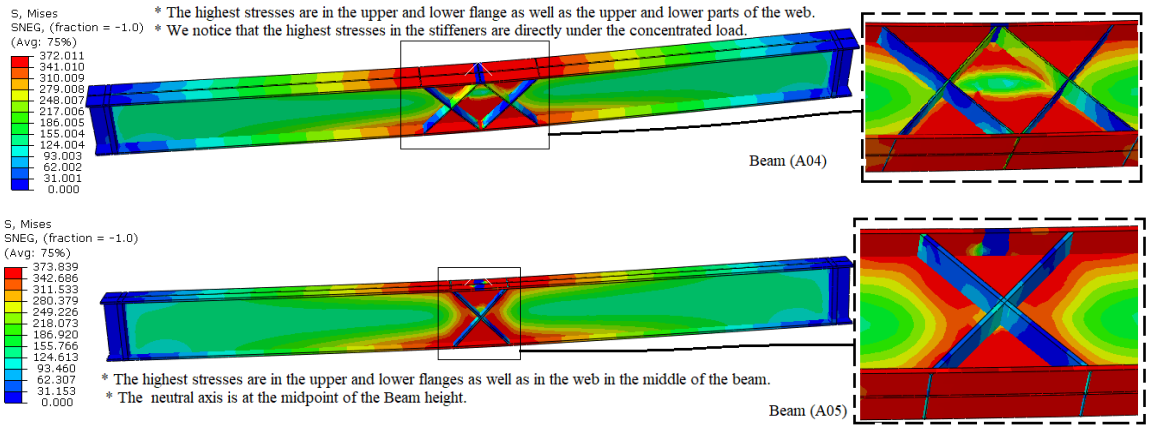

Figure 6. The deformation and stresses in beams at yielding load

Table 3 illustrates that the yield load value is lowest for the reference beam at 157.424, whereas beam A05 exhibits the maximum yield load at 172.547, reflecting an increase of 9.6%. The vertical deflection values for all beams vary from 17.25 mm for beam (A03) to 19.78125 mm for beams (A02) and (A04). It is observed that in all beams with stiffeners; stresses originate from the web and flange. The stress distribution in the flange and web indicates that the stress levels in the stiffeners are comparatively low at this point.

4.4. Effect Strengthen the Beams by Stiffeners on Ultimate Stress in Beams

In beam A0, it is observed that the formation of a sunken area in the upper flange where it is exposed to direct load results in undulation, as shown in Figure 7. As for beam A01, we notice the beginning of a local buckling of the upper flange on both sides of the vertical stiffener. As for beam A02, at this stage, the beginning of the local buckling occurs in the upper flange, and we notice that the stress values in the stiffeners are much higher than in beam A01.

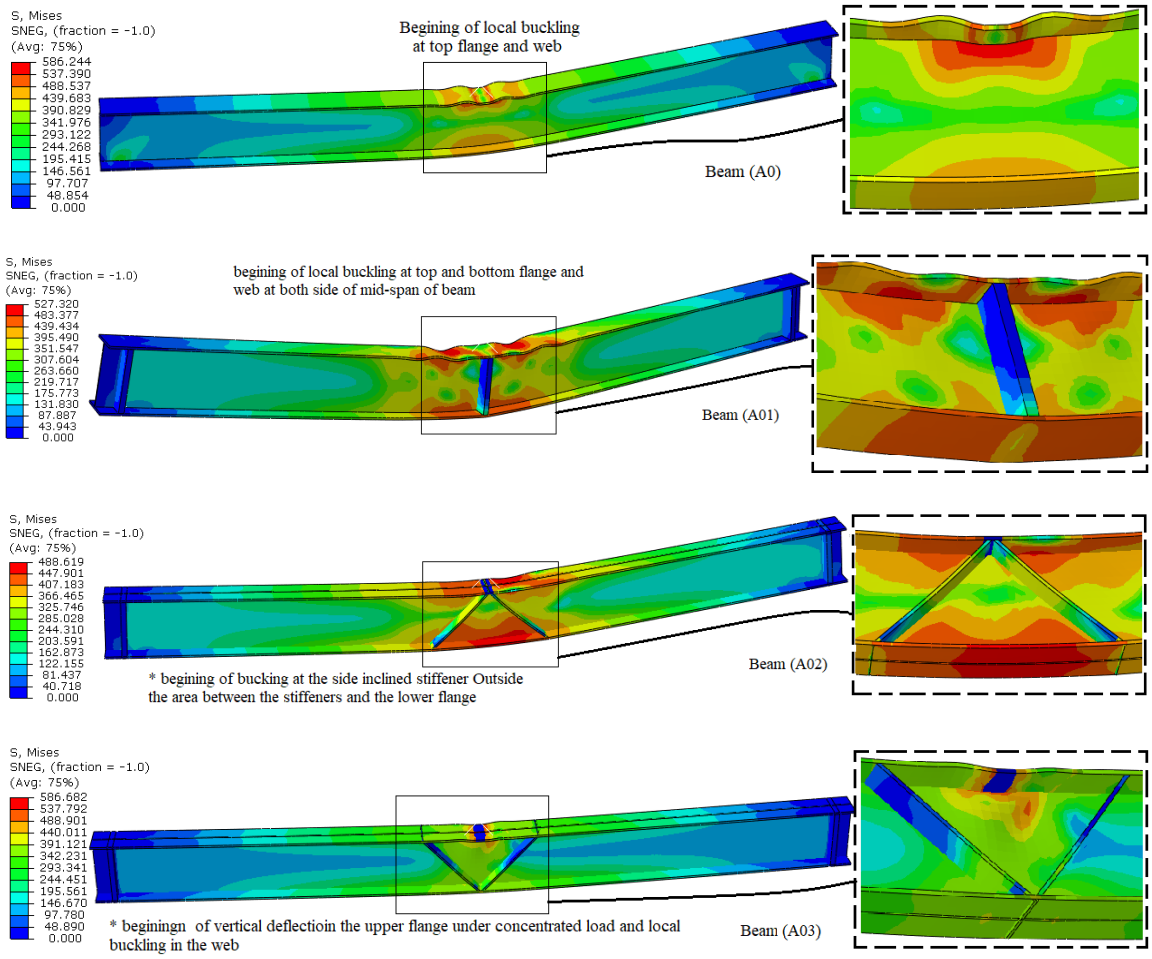

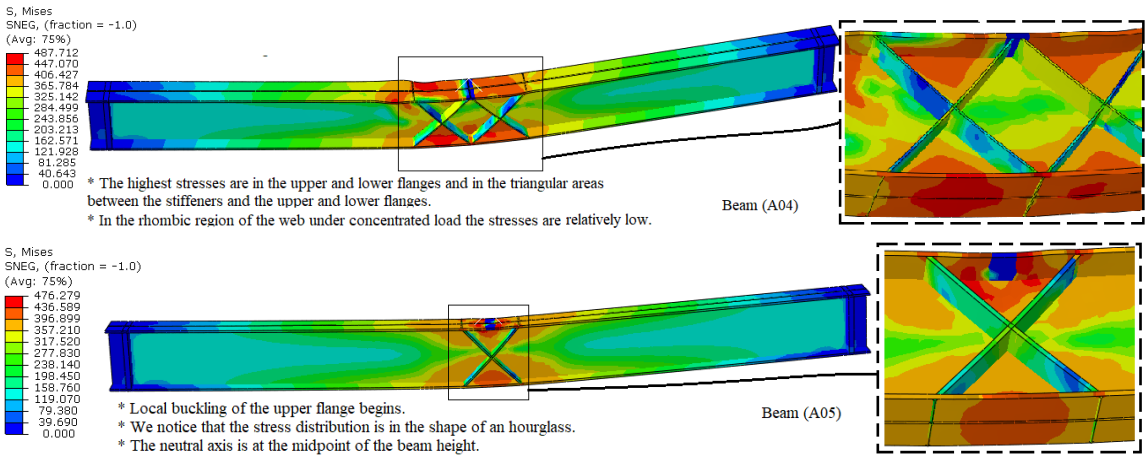

Figure 7. The deformation and stresses in beams at ultimate load

As for the A03 beam, it reaches its maximum load with a relatively low vertical deflection compared to the other beams (40 mm). As with the reference beam, the initial subsidence occurs in the area exposed to the direct load. The lower stiffeners' stresses are much higher than the upper ones. The lower part starts from the beam's middle and connects to the flange, where the stresses are highest. The lower part of the stiffeners has much higher stresses than the upper part because it starts in the middle of the beam and connects to the flange, where the stresses are the highest. As for beam A04, we notice that the stress values are relatively large in the triangles enclosed between the stiffeners and the upper and lower flanges, while in the rhombic-shaped region located in the middle, the stresses are relatively small. We also notice that the deformation is relatively small, with only a slight undulation in the upper flange. As for beam A05, we note that the stresses are greatest under concentrated load in the upper flange and the web in the area between the inclined stiffeners and the upper flange.

According to Table 3, beam (A03) has the lowest ultimate load value (170.269 kN), whereas beam (A04) has the ultimate load (201.736 kN), which is an increase of 10.28% above reference beam (A0). It is observed that in all beams with stiffeners; stresses originate from the flange and increase toward the web. At this stage, it may be seen that the stress distribution in the flange and web is observed, with the stress levels in the stiffeners being comparatively low at this point. Deformation in the beams can also be clearly observed.

4.5. Effect Strengthen the Beams by Stiffeners the Stresses and Deformation in Beams at Failure Load (at Vertical Deflection = 300 mm)

Figure 8 illustrates the beams experiencing a vertical deflection of 300 mm, corresponding to a plastic rotation angle of 0.2 rad, which indicates the model's attainment of sectional failure. Beam A0 exhibits a sunken upper flange, resulting in considerable buckling of the web. Beam A01 exhibits double local buckling in the upper flange, alongside buckling in the web on both sides of the vertical stiffener. Beam A02 exhibits distortional buckling throughout its entire section, particularly in the region outside the delta adjacent to the inclined stiffeners. This phenomenon occurs as if the stiffeners are exerting stresses beyond the triangular area defined by the stiffeners on two sides and the lower flange on the third side. Beam A03 exhibits concentrated stresses at the midpoint due to the inclined stiffeners, resulting in subsidence of the upper flange and significant buckling in the web. The A04 beam, characterized by a double X, exhibits buckling throughout the section at the edges of the stiffeners, along with noticeable distortion in the stiffeners themselves. In beam A05, buckling is observed in the upper flange, the web directly beneath it, and at both ends of the X-stiffeners.

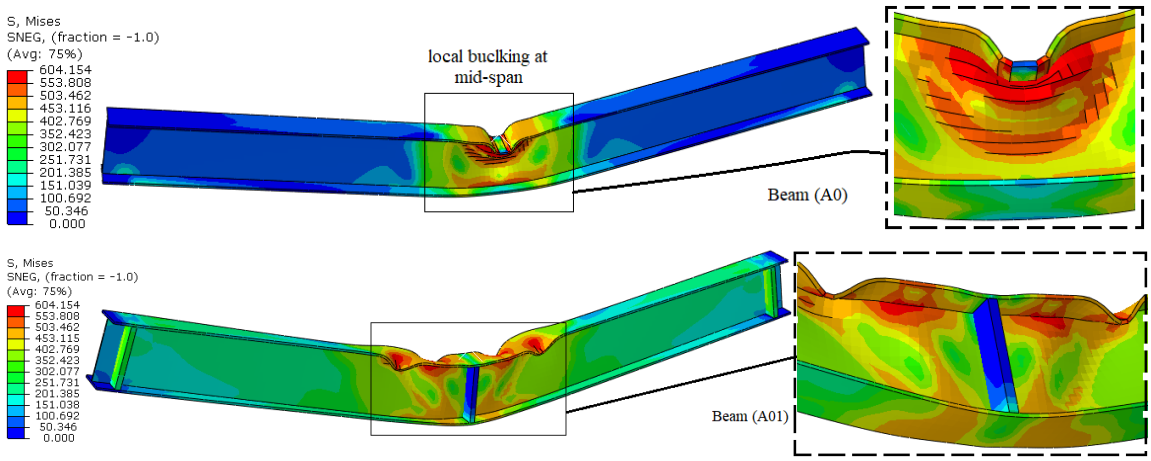

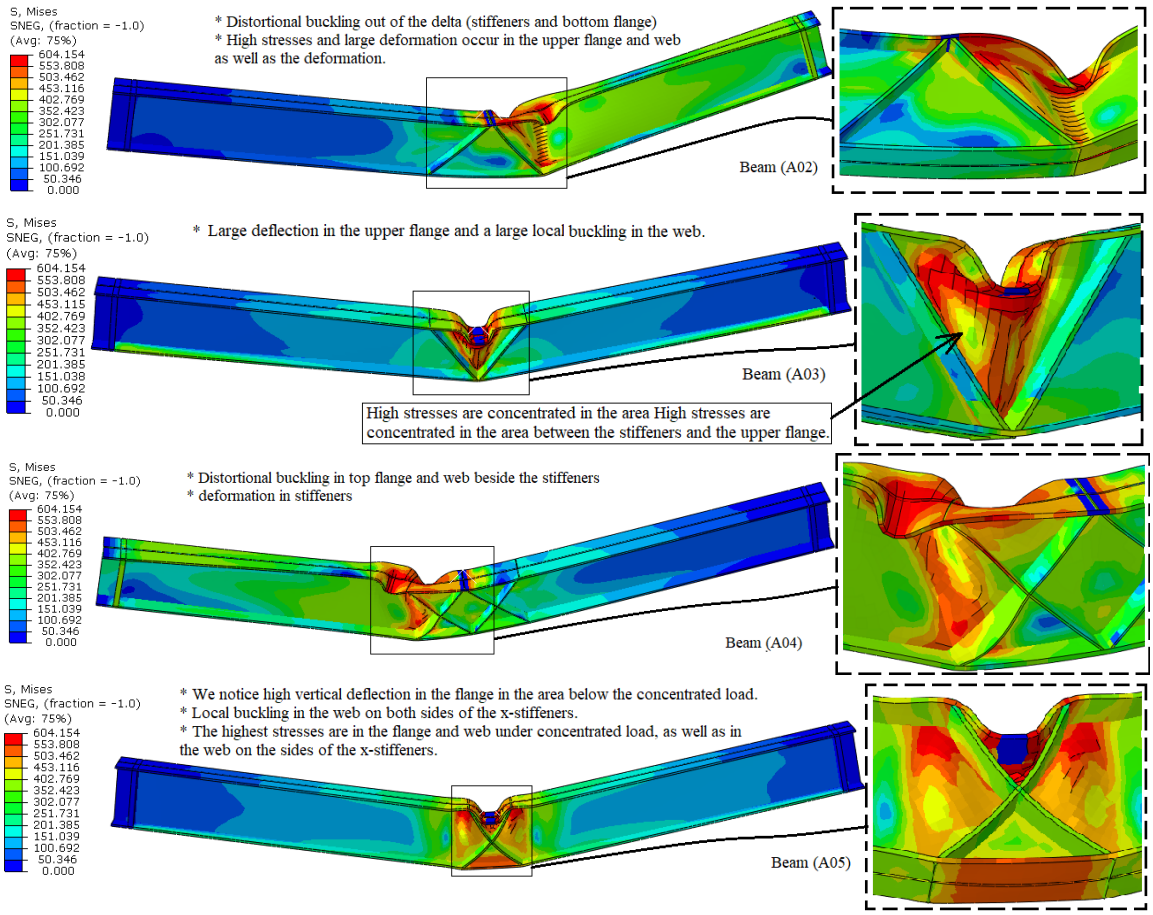

Figure 8. The deformation and stresses in I-steel beams at vertical displacement =300mm

5. Conclusions

Using Abaqus to analyze beam behavior can yield positive results, providing an indication of the type of stiffeners that can guide us toward the best stiffeners. It also reduces the number of models required, allowing for laboratory testing of only those that yield positive results. It also provides a clearer picture of stiffener behavior during loading and until failure. Therefore, we can conclude the following:

- It is essential to install a vertical stiffener beneath the concentrated load, as demonstrated in beam (A01), or to employ a reinforcement configured as an inverted "V," as seen in beam (A02), or to utilize a double "X" reinforcement, as illustrated in beam (A04), to avert or delay the buckling of the upper flange and web.
- The stress values in beams (A02) and (A05) are significantly elevated adjacent to the stiffeners, while deformation is pronounced in the flange and web, indicating the formation of a plastic hinge. This suggests that the stiffeners effectively reinforced the central region of the beam, making the adjacent areas relatively weak compared to the region between the stiffeners.
- The "V" shaped stiffener clearly confines stresses inside the central region of the beam (the area between the two stiffeners and the upper flange), resulting in a quick and abrupt failure of the beam; hence, this reinforcing type is considered to be passive.
- The first loading phase demonstrates that the use of stiffeners lowers the stresses in the web, hence postponing the attainment of the yield load, and subsequently the ultimate load and final collapse.
- In beam (A04, A05), there was an increase in the yield load, as it showed an increase of 9.6% compared to the reference beam (A0).
- The beam (A04) is regarded as the superior option in the area from the yield point to the ultimate load, exhibiting an increase of 10.28% relative to the reference beam (A0).
- The beam (A05) is regarded as the most performing following the ultimate load stage till failure, exhibiting an increase rate of 102.5% compared to the reference beam (A0).
- Many traditional structural design methodologies, including Allowable Stress Design, Working Stress Design, and Elastic Analysis, depend on the structure being beyond its yield point, therefore functioning only inside the

elastic domain. All reinforced beams exhibited an enhancement in the area under the curve (elastic region), particularly beams A2 and A4, which showed an increase of around 70% relative to the reference beam.

- Numerous contemporary structural design methodologies, including Ultimate Strength Design (USD), Load and Resistance Factor Design (LRFD), Plastic Design, and Ductility-based Design, are predicated on the region from yield to ultimate load. The beam (A2) exhibited an approximate 25% increase relative to the reference beam.
- The area under the curve from maximum load to failure indicates the component's capacity to retain ductility and absorb energy post-maximum load. It is a critical element in seismic design, evaluating safety against abrupt failure and choosing materials that demonstrate significant deformation prior to failure.

6. Notations

Es	Modulus of elasticity	ν_s	Passion's ratio
IX-X	Moment of inertia about x-axis	Iy-y	Moment of inertia about y-axis
P	Concentrated one point load	Pu	Ultimate load
Py	Yield load	MP	Plastic moment
Z	Plastic section modulus	Ai	Area in elastic section
yi	Centroidal distance from the neutral axis	r	Radius of curvature
σ_s	stress in steel beam	Ɛ	Strain
$Ɛsh$	Strain hardening strain	$Ɛu$	Strain at ultimate stress
$Ɛy$	Yield strain	Fy	Yield strength of material
Fu	Ultimate strength of material	θp	The plastic joint rotation
δy	Vertical displacement in elastic region	δp	Vertical displacement in plastic region

7. Declarations

7.1. Author Contributions

Conceptualization, A.F.A. and M.A.R.; methodology, A.F.A. and A.K.K.; software, A.F.A.; validation, A.F.A. and Z.A.H.; formal analysis, A.F.A. and M.A.R.; investigation, A.F.A. and Z.A.H.; resources, A.F.A. and Z.A.H.; writing—original draft preparation, M.H.A. and N.S.T.; writing—review and editing, M.H.A. and N.S.T.; visualization, A.F.A.; supervision, A.F.A.; project administration, A.F.A. and M.A.R.; funding acquisition, A.F.A. and A.K.K. All authors have read and agreed to the published version of the manuscript.

7.2. Data Availability Statement

The data presented in this study are available in the article.

7.3. Funding

The authors received no financial support for the research, authorship, and/or publication of this article.

7.4. Conflicts of Interest

The authors declare no conflict of interest.

8. References

[1] Subramanian, N. (2010). Steel structures: design and practice. Oxford University Press, Oxford, United Kingdom.

[2] Atshan, A. F., Rasheed, M., Mahmoud, K. S., & Al Sharify, Z. T. (2024). Yielding Behaviour of Steel Beams as a Result of the Shape of the Strands' Fixity Profile. Tikrit Journal of Engineering Sciences, 31(3), 221–232. doi:10.25130/tjes.31.3.21.

[3] Yang, Y., & Lui, E. M. (2012). Behavior and design of steel I-beams with inclined stiffeners. Steel and Composite Structures, 12(3), 183–205. doi:10.12989/scs.2012.12.3.183.

[4] Prabha, G., & Emilrevan, R. (2018). Flexural Behavior of Rolled Steel I Beam with Different Stiffener Position. International Journal of Engineering & Technology, 7(4.2), 10. doi:10.14419/ijet.v7i4.19992.

[5] AL-Ridha, A. S. D., Abbood, A. A., & Atshan, A. F. (2020). Evaluating the Efficiency of Strengthening Hot-Rolled I-Sectioned Steel Beams by using Additional Plates and Inclined Stiffeners with Various Widths. IOP Conference Series: Materials Science and Engineering, 870(1), 12102. doi:10.1088/1757-899X/870/1/012102.

[6] Al-Ridha, A. S. D., Atshan, A. F., Mahmoud, K. S., & Hameed, Q. K. (2019). Effect of strengthening of steel beams with variable length by using carbon fiber. Journal of Engineering (United Kingdom), 2019, 1631692. doi:10.1155/2019/1631692.

[7] Al-Ridha, A. S. D., Hameed, Q. K., Atshan, A. F., Abbood, A. A., & Dheyab, L. S. (2020). Evaluation of strengthening steel beams using the technique of carbon fiber confinement by a steel plate (CFCSP). Advances in Civil Engineering Materials, 9(1), 53–66. doi:10.1520/ACEM20190164.

[8] Yam, M. C. H., Ma, H., Lam, A. C. C., & Chung, K. F. (2011). Experimental study of the strength and behaviour of reinforced coped beams. Journal of Constructional Steel Research, 67(11), 1749–1759. doi:10.1016/j.jcsr.2011.04.015.

[9] Siwowski, T. W., & Siwowska, P. (2018). Experimental study on CFRP-strengthened steel beams. Composites Part B: Engineering, 149, 12–21. doi:10.1016/j.compositesb.2018.04.060.

[10] Peiris, A., & Harik, I. (2021). Steel beam strengthening with UHM CFRP strip panels. Engineering Structures, 226, 111395. doi:10.1016/j.engstruct.2020.111395.

[11] Qadir, S. J., Nguyen, V. B., & Hajirasouliha, I. (2024). Design optimisation for cold rolled steel beam sections with web and flange stiffeners. Journal of Constructional Steel Research, 213, 108375. doi:10.1016/j.jcsr.2023.108375.

[12] Huovinen, S. (1997). Action of glued steel plates in strengthening of structures. Nordic concrete research, Scandic Park Sandefjord, Norway.

[13] Sallam, H. E. M., Saba, A. M., Mamdouh, W., Maaly, H., & Ibrahim, I. (2005). Strengthening of Steel Beams Using Bonded Cfrp and Steel Plates: a Pilot Study. Al-Azhar University Engineering Journal, 8(10), 23–29.

[14] Haghani, R., Al-Emrani, M., & Kliger, R. (2009). Interfacial stress analysis of geometrically modified adhesive joints in steel beams strengthened with FRP laminates. Construction and Building Materials, 23(3), 1413–1422. doi:10.1016/j.conbuildmat.2008.07.013.

[15] Yossef, N. M. (2015). Strengthening Steel I-Beams by Welding Steel Plates before or While Loading. International Journal of Engineering Research & Technology, 4(07), 545-550.

[16] Demir, A., Ercan, E., & Demir, D. D. (2018). Strengthening of reinforced concrete beams using external steel members. Steel and Composite Structures, 27(4), 453–464. doi:10.12989/scs.2018.27.4.453.

[17] Chen, C. C., & Sudibyo, T. (2018). Effect of Intermediate Stiffeners on the Behaviors of Partially Concrete Encased Steel Beams. Advances in Civil Engineering, 2018(1), 8672357. doi:10.1155/2018/8672357.

[18] Yang, J., Wadee, M. A., & Gardner, L. (2025). Strengthening of steel I-section beams by wire arc additive manufacturing — Concept and experiments. Engineering Structures, 322, 119113. doi:10.1016/j.engstruct.2024.119113.

[19] Yuan, F., Chen, M., & Pan, J. (2020). Flexural strengthening of reinforced concrete beams with high-strength steel wire and engineered cementitious composites. Construction and Building Materials, 254, 119284. doi:10.1016/j.conbuildmat.2020.119284.

[20] Karande, S. V, & Angalekar, S. S. (2016). Study of nonlinear static finite element analysis and plastic behaviour of steel beam section. International Research Journal of Engineering and Technology, 3(7), 196-1969.

[21] Truong, V. H., Papazafeiropoulos, G., Pham, V. T., & Vu, Q. V. (2019). Effect of multiple longitudinal stiffeners on ultimate strength of steel plate girders. Structures, 22, 366–382. doi:10.1016/j.istruc.2019.09.002.

[22] Han, L. H., Wang, W. Da, & Zhao, X. L. (2008). Behaviour of steel beam to concrete-filled SHS column frames: Finite element model and verifications. Engineering Structures, 30(6), 1647–1658. doi:10.1016/j.engstruct.2007.10.018.

[23] Gardner, L., Li, J., Meng, X., Huang, C., & Kyvelou, P. (2024). I-section steel columns strengthened by wire arc additive manufacturing - concept and experiments. Engineering Structures, 306, 117763. doi:10.1016/j.engstruct.2024.117763.

[24] Jagtap, P., Pore, S., & Jagtap, M. (2025). Comparative study of steel I-beam strengthened with CFRP and steel plate as a web stiffeners. Next Materials, 9, 101064. doi:10.1016/j.nxmate.2025.101064.

[25] Yang, J., Wadee, M. A., & Gardner, L. (2025). Strengthening of hot-rolled S355 steel I-section beams using WAAM high strength steel. Thin-Walled Structures, 215. doi:10.1016/j.tws.2025.113437.

[26] Xie, W., Iranpour, A., & Mohareb, M. (2025). Elastic Lateral Torsional Buckling Resistance of I-Beams Strengthened with Side Plates. Journal of Structural Engineering, 151(9). doi.org/10.1061/jsendh.steng-14512.

[27] Salmon, C.G., Johnson, J.E. & Malhas, F.A. (2009) Steel Structures: Design and Behavior (5th Ed.), Pearson Prentice Hall, Old Bridge, United States.

[28] Timoshenko, S. P., & Gere, J. M. (1972). Mechanics of Materials. McGraw-Hill, Columbus, United States.

[29] Chen, W. F., & Sohal, I. (1995). Plastic Design and Second-Order Analysis of Steel Frames. In Plastic Design and Second-Order Analysis of Steel Frames. Springer, New York, United States. doi:10.1007/978-1-4613-8428-1.

[30] FEMA 440. (2005). Improvement of nonlinear static seismic analysis procedures. Federal Emergency Management Agency. Washington, United States.

[31] Yun, X., & Gardner, L. (2017). Stress-strain curves for hot-rolled steels. Journal of Constructional Steel Research, 133, 36–46. doi:10.1016/j.jcsr.2017.01.024.